Physics Letters A 382 (2018) 2952–2958

Contents lists available at ScienceDirect

Physics Letters A

www.elsevier.com/locate/pla

Topological phases in Bi/Sb planar and buckled honeycomb monolayers

N. Nouri [a,b,*], M. Bieniek [a], M. Brzezińska [a], M. Modarresi [c,d], S. Zia Borujeni [e], Gh. Rashedi [b], A. Wójs [a], P. Potasz [a]

[a] Department of Theoretical Physics, Faculty of Fundamental Problems of Technology, Wrocław University of Science and Technology, 50-370 Wrocław, Poland
[b] Department of Physics, Faculty of Sciences, University of Isfahan, Isfahan 81746-73441, Iran
[c] Laboratory of Organic Electronics, Department of Science and Technology, Linkoping University, 60174 Norrkoping, Sweden
[d] Department of Physics, Ferdowsi University of Mashhad, Mashhad, Iran
[e] Department of Mathematics, Tehran Central Branch, Islamic Azad University, Tehran, Iran

ARTICLE INFO

Article history:
Received 12 February 2018
Received in revised form 26 April 2018
Accepted 20 June 2018
Available online 25 June 2018
Communicated by R. Wu

Keywords:
Topological insulators
Bismuth
Antimony

ABSTRACT

We investigate topological phases in two-dimensional Bi/Sb honeycomb crystals considering planar and buckled structures, both freestanding and deposited on a substrate. We use the multi-orbital tight-binding model and compare results with density functional theory calculations. We distinguish topological phases by calculating topological invariants, analyzing edge states properties of systems in a ribbon geometry and studying their entanglement spectra. We show that coupling to the substrate induces transition to the Z_2 topological insulator phase. It is observed that topological crystalline insulator (TCI) phase, found in planar crystals, exhibits an additional pair of edge states in both energy spectrum and entanglement spectrum. Transport calculations for TCI phase suggest robust quantized conductance even in the presence of crystal symmetry-breaking disorder.

© 2018 Elsevier B.V. All rights reserved.

1. Introduction

Novel topological phases have gained an immense interest of both experimentalists and theorists in the current decade [1–11] due to attractive potential technological applications in spintronic and quantum computing devices [12]. Topological insulators exhibit the energy gap inside the bulk and conduction channels at the edges, inherently protected against certain types of scattering. Quantum spin Hall (QSH) systems are two-dimensional (2D) representatives of the family of Z_2 topological insulators protected by time-reversal symmetry [13]. Topologically nontrivial energy gap is usually inverted by large spin–orbit coupling (SOC), which is a characteristic of heavy elements. QSH systems were experimentally observed in thickness-tunable quantum wells and honeycomb-like systems based on groups of IV [14–16], II–VI [17,18], III–V [19–23] and V [24–27] elements including heavy atoms like bismuth or antimony. Recently, thin films of topological insulators protected by crystalline symmetries were recognized and dubbed topological crystalline insulators [6–11].

Bi and Sb crystals were extensively studied in the context of their topological properties [24,28–38,26,39,32,40,27,41–47,31,43,8]. Murakami [24] has predicted that Bi bilayer is Z_2 topological insulators with helical edge modes propagating in opposite directions. This fact was later confirmed experimentally by scanning tunneling microscopy measurements [28–31]. Several authors investigated robustness of topological properties of Bi(111) and Sb(111) bilayers and few bilayer crystals [32–38]. Sb(111) thin films with less than four bilayers were shown to be topologically trivial [26]. Transitions between topologically trivial and nontrivial phases can be induced by structure modifications involving chemical methods [39], artificial variation of spin–orbit coupling in Bi [32,40], strain [27,41–44] or interaction with a substrate [45–47,31,43]. Recently, TCI phase in flat Bi and Sb honeycomb layers was predicted [8]. In the presence of strain, buckled structures become completely flat, which leads to the formation of bismuthene and antimonene, for Bi and Sb composed crystals, respectively.

In the following work, we investigate various topological phases in planar and buckled Bi and Sb two-dimensional honeycomb layers using multi-orbital tight-binding (TB) model and compare results with density functional theory (DFT) calculations. We analyze whether TB method can be used as a complementary tool to characterize these crystals, as it allows to study larger systems. We distinguish different topological phases for freestanding structures and those deposited on a substrate. These phases are identified by computing topological invariants, examining band structures in a ribbon geometry and analyzing their entanglement spectra (ES).

* Corresponding author at: Department of Physics, Faculty of Sciences, University of Isfahan, Isfahan 81746-73441, Iran.
E-mail address: nafise.nour@sci.ui.ac.ir (N. Nouri).

https://doi.org/10.1016/j.physleta.2018.06.037
0375-9601/© 2018 Elsevier B.V. All rights reserved.

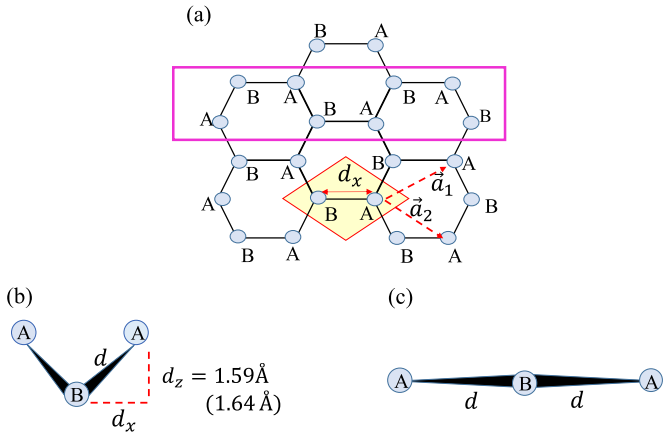

Fig. 1. (a) Top view of a honeycomb crystal structure. $\vec{a}_1$ and $\vec{a}_2$ are the lattice vectors. Rhomboid denotes a unit cell of infinite layer, whereas rectangle corresponds to the zigzag nanoribbon unit cell with periodic boundary conditions in a vertical direction. The atoms from a infinite layer unit cell are labeled as A and B. (b) Side view of bismuth and antimony bilayers. In our TB method, we set the out of plane distortion to $d_z = 1.58$ Å for bismuth and $d_z = 1.64$ Å for antimony. d is the bond length between the nearest neighboring atoms. (c) Corresponding side view of bismuthene and antimonene with interatomic distance d.

We focus mainly on characteristic features of TCI phase and study its topological protection against scattering by calculating conductance in the presence of crystal symmetry-breaking disorder.

The paper is organized as follows. In Section 2 we introduce the methodology. Results from tight-binding method and density functional theory calculations during buckled-flat transitions of freestanding systems are compared in Section 3. In Section 4, we analyze the effect of the interaction with the substrate. In Section 5 we characterize topological phases using entanglement spectrum and in Section 6 transport properties of TCI phase are studied. The results are concluded in Section 7.

2. Methods

2D crystals composed of Bi and Sb are schematically shown in Fig. 1(a). A hexagonal unit cell contains two atoms, denoted by A and B. Freestanding Bi and Sb honeycomb layers have the lowest energy when two atoms are displaced in a direction perpendicular to a lattice plane, thus they are usually called bilayers [24]. While this displacement slightly differs in a literature depending on type of calculations [43,48,49], in our TB method we take $d_z = 1.58$ Å for Bi and $d_z = 1.64$ Å for Sb. We will consider transitions between buckled Bi and Sb bilayers, Fig. 1(b), to flat honeycomb crystals, bismuthene and antimonene (see Fig. 1(c)) caused by an external uniform strain.

2.1. Tight-binding model

We use four-orbital (s, p_x, p_y, p_z) TB method with parametrization introduced by Liu and Allen [50] for bulk bismuth and antimony. The inter-atomic hopping up to the next nearest-neighbors and the atomic spin–orbit coupling (SOC) are parametrized with the Slater–Koster approach [51]. Therefore, we can write Hamiltonian as

$$\begin{aligned} H = & \sum_{\alpha,\sigma,R} |\alpha,\sigma,R\rangle E_\alpha \langle\alpha,\sigma,R| \\ & + \sum_{\alpha,\beta,\sigma,R,R'} \left[|\alpha,\sigma,R\rangle V^{\mathrm{I}}_{\alpha\beta} \langle\beta,\sigma,R'| + H.c \right] \\ & + \sum_{\alpha,\beta,\sigma,R,R''} \left[|\alpha,\sigma,R\rangle V^{\mathrm{II}}_{\alpha\beta} \langle\beta,\sigma,R''| + H.c \right] \\ & + \tfrac{\lambda}{3} \sum_{\alpha,\beta,\sigma,\sigma',R} \left[|\alpha,\sigma,R\rangle \vec{L}\cdot\vec{\sigma} \langle\beta,\sigma',R| + H.c \right], \end{aligned} \tag{1}$$

Table 1
Bismuth and antimony two-center hopping integrals taken from Refs. [42]**, [53]*, [50]. a is a lattice constant, and d_x and d_z denote parallel and perpendicular (buckling) distance between nearest-neighbor atoms in a honeycomb lattice, indicated in Fig. 1(b).

Parameter (eV)	Bi	Sb	Parameter (eV)	Bi	Sb
E_s	−10.906	−10.068	$V^{\mathrm{I}}_{pp\sigma}$	1.854	2.342
E_p	−0.486	−0.926	$V^{\mathrm{I}}_{pp\pi}$	−0.600	−0.582
$V^{\mathrm{I}}_{ss\sigma}$	−0.608	−0.694	$V^{\mathrm{II}}_{pp\sigma}$	0.156	0.352
$V^{\mathrm{I}}_{sp\sigma}$	1.320	1.554	λ	1.5	0.6
a (Å)	4.53	4.30	d_z (Å)	1.58*	1.64**
d_x (Å)	2.62	2.48			

where $\{\alpha, \beta\}$ label orbital $\{s, p_x, p_y, p_z\}$ and $\{\sigma, \sigma'\}$-spin degrees of freedom. $R'(R'')$ denote atomic positions of the nearest, (next-nearest) neighbors to an atom localized at R. E_α corresponds to the on-site energies and $V_{\alpha\beta}$ are Slater–Koster two-center integrals between α and β orbitals (I for nearest and II for next-nearest neighbors). The last term describes the spin–orbit coupling with strength λ. TB parameters are listed in Table 1. 1/3 factor is introduced to renormalize atomic SOC strength λ in order to obtain correct SOC splitting of the valence band [52]. Buckled-flat crystal transitions are modeled by linearly decreasing d_z and at the same time linearly increasing lattice constants of Bi and Sb bilayers up to the values corresponding to completely flat bismuthene and antimonene, with $a = 5.35$ Å and $a = 5.00$ Å, respectively. According to Ref. [31], the effect of SiC substrate is effectively described by shifting p_z orbitals away from the low-energy sector.

2.2. Density functional theory

We study the atomic configurations and electronic properties of relaxed and strained 2D Sb and Bi crystals in the DFT framework. The DFT calculations are done within the generalized gradient approximation (GGA) and the Perdew–Burke–Ernzerhof (PBE) [54] exchange correlation function. The core electrons were model using the norm-conserving pseudo potentials. The cut-off energy for the plane wave expansion and charge density calculations are set to 75/85 Ry and 750/850 Ry respectively for Sb/Bi 2D layers. We note that while usually the ratio between the charge density cutoff to the wave function cutoff is four, here the use of gradient-corrected functional and for pseudopotential without non-linear core correction requires a higher ratio value in order to reach energy convergence with 1 meV/10 meV for Sb/Bi monolayer, respectively. The distance between layers is set to 15 Å to avoid interaction between adjacent image layers. We apply the biaxial tensile strain which saves the hexagonal shape of the relaxed unit cell. The first Brillouin zone integration is performed in the Monkhorst–Pack algorithm [55] using a $15 \times 15 \times 1$ k-grid for relaxation of strained atomic configurations. In the relaxation, the total force on each atom in the final configuration is less than 0.001 (Ry/au). We start DFT relaxation from a completely flat structure and a buckled one to compare the final energy and find the lowest energy configuration. For band structure calculations which include the SOC, we used fully-relativistic pseudo potentials and a fine mesh of $25 \times 25 \times 1$ for k-grid. All DFT calculations presented in this article were performed using the Quantum-Espresso package [56].

The relaxed Bi and Sb honeycomb lattices are buckled and with lattice constants $a = 4.45$ Å and $a = 4.13$ Å, respectively. The equilibrium buckling of relaxed structures are $d_z = 1.64$ Å for Sb and $d_z = 1.69$ Å for Bi 2D planes. Resulting atomic configurations are in a good agreement with previous reports [57,58]. Obtained values differ from chosen tight-binding parameters by less than 10%, and we verify that this discrepancy does not affect results in a qualitative way.

2.3. Entanglement spectrum

Entanglement measures have provided a new insight into characterization of quantum phases of matter. Having a composite system S divided into two parts I and II with the total Hilbert space $\mathcal{H}_S = \mathcal{H}_I \otimes \mathcal{H}_{II}$, the reduced density matrix ρ_I corresponding to the subsystem I is obtained by tracing out degrees of freedom associated with the part II. Complexity of the ground state can be quantified by the von Neumann entanglement entropy defined as $S_I = -\mathrm{Tr}\rho_I \log \rho_I$. In Ref. [59], it was shown that singular value decomposition (or Schmidt decomposition in a quantum information theory language) of a state allows to identify topologically non-trivial systems. Since $\rho_I \geq 0$, it can be rewritten as a $\rho_I = \exp(-H_I)/Z_I$, where Z_I is a partition function ensuring that $\mathrm{Tr}\rho_I = 1$. H_I is called the entanglement Hamiltonian and a set of its eigenvalues $\{\xi\}$ is known as the entanglement spectrum.

When system is bilinear in creation and annihilation operators (i.e. free-fermionic), entanglement spectrum can be evaluated through two-point correlation function [60]. For a translationally-invariant Hamiltonian given in the momentum space $H(k)$ with a many-body ground state $|GS\rangle = \prod_{nk} a^\dagger_{nk}|0\rangle$ build from n occupied single-particle Bloch states, the correlation matrix is computed by using the following formula

$$C^{\alpha\beta}_{ij}(k) = \langle GS|c^\dagger_{i\alpha k}c_{j\beta k}|GS\rangle \tag{2}$$

for each momentum sector k separately. Indices i, j are labeling lattice sites, while α, β-spin and orbital degrees of freedom. A relation between spectrum of C denoted by $\{\zeta\}$ and entanglement spectrum is $\zeta = (1 + \exp(\xi))^{-1}$, hence from now we refer to eigenvalues of C as the single-particle entanglement spectrum [61,62].

Topological properties of the system are revealed in the structure of the spectrum of $C(k)$. C is a Hermitian matrix, $C = C^\dagger$, and can be seen as a spectrally flattened original Hamiltonian sharing the same symmetries as well. The single-particle entanglement spectrum is bounded by 0's and 1's, with eigenvalues equal to one (zero) corresponding to fully occupied (unoccupied) states. If the system is in a topologically non-trivial phase, intermediate eigenvalues connecting 0's and 1's called the spectral flow are observed [61]. Moreover, the presence of midgap states (exactly at $\zeta = 1/2$) is associated with inversion symmetry in the system [62,63]. Our aim is to observe whether distinct features in entanglement spectra of TI and TCI phases are present.

2.4. Transport calculations

In transport calculations we consider two-terminal geometry with semi-infinite leads attached to the left and the right edge of the scattering region. We use the Landauer approach for the differential conductance $G = e^2h^{-1}T$, where T is transmission matrix calculated using recursive Green's functions approach, as explained in our previous work [32]. Disorder effects were introduced using Anderson model with on-site values chosen randomly from a uniform distribution $[-W/2, W/2]$ (with W being the disorder strength) and the conductance averaged over 100 samples with the different impurity realizations. All transport results were calculated for the nanoribbon scattering region size $N = 50 \times 100$ atoms without the inclusion of strain in flat system due to its negligible effect on a qualitative picture.

3. Comparison between density functional theory and tight-binding results for freestanding structures

First-principles methods are commonly used in order to study electronic properties of Bi and Sb honeycomb 2D crystals [24,27,28,30–37,26,39–43,8]. We justify applicability of TB model by comparing results with our DFT calculations. We focus on topological properties of the systems in a presence of biaxial strain leading to a transition between buckled and flat structures. Strain in TB method is modeled by linearly decreasing d_z and at the same time linearly increasing lattice constants of Bi and Sb bilayers up to the values corresponding to completely flat structures, bismuthene and antimonene. Z_2 topological invariant characterizing TIs is calculated from the parities of filled bands at four time-reversal invariant momentum (TRIM) points [3], while mirror Chern numbers for TCI phase using a method from Ref. [6]. Fig. 2 shows phase diagrams obtained within TB and DFT methods for Bi in (a) and (b) as well as for Sb in (c) and (d). Strain leads to gap closing and reopening around 13% as shown in Fig. 2 (a). When the system is completely flat for 20% strain, TCI phase is seen, as expected in bismuthene [8]. In case of DFT, we notice that after a critical value of strain 16%, the system relaxes to the flat structure exhibiting TCI phase, which has the lowest energy. One can also notice the energy gap closing point around 5% strain in Fig. 2 (b), however we verify that the system remains in TI phase. This feature is not observed in TB results, however topological phases are correctly predicted. Qualitative agreement between phase diagrams obtained by TB and DFT methods is observed for Sb 2D honeycomb crystal. Strain induces a transition from a trivial phase to TI at around 12% in DFT and around 5% in TB. For 22% strain (not shown) in DFT method the structure becomes flat and we see a semi-metallic phase, similarly to results from Ref. [8], and in our TB results between 13%–16% strain. In Ref. [8], TCI phase was observed for a flat structure with strain larger than 25% and we see TCI in our TB, but we did not consider such strain in our DFT studies.

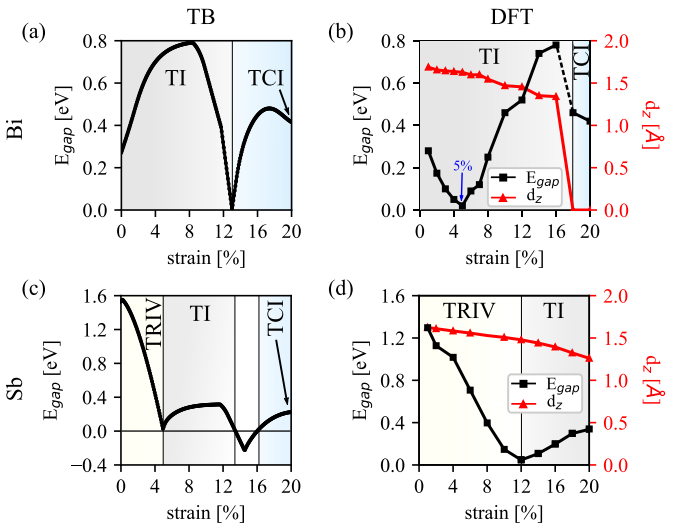

Fig. 2. Energy band gap E_{gap} as a function of strain for structures in the vacuum for Bi (a, b) and Sb (c, d) crystals. (a) and (c) show tight-binding results, while (b) and (d) – DFT results. Distinct topological phases are marked by different colors. 20% strain corresponds to the flat structure exhibiting TCI phase in case of Bi.

4. Substrate effect within tight-binding method

We investigate the effect of interaction between Bi and Sb 2D crystals with SiC substrate within TB method. Deposited samples are coupled to SiC mainly through orbitals perpendicular to the layer, p_z in this case. This can be modeled by shifting away the p_z orbital energy E_{p_z} from a low-energy part of spectrum [31]. We note that within this effective model describing the substrate effect it is not possible to determine a position of the Fermi energy at intermediate values of E_{p_z}, when energy bands continuously shift in energy with E_{p_z}. In Fig. 3 (yellow area) around $E_{p_z} = -2$ eV, we

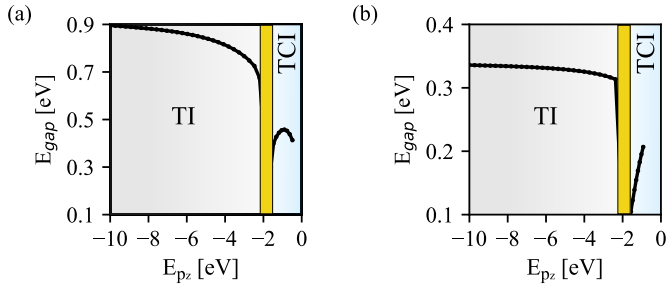

Fig. 3. Energy band gap E_{gap} as a function of interaction with a substrate modeled by changing of energy E_{p_z} of p_z orbitals for (a) bismuthene and (b) antimonene. $E_{p_z} = -0.486$ eV in (a) and $E_{p_z} = -0.926$ eV in (b) correspond to freestanding bismuthene (antimonene), see Table 1, and $E_{p_z} = -10$ eV to structures deposited on the substrate. The yellow areas refer to E_{p_z} values with not well defined Fermi energy (see the main text), coinciding with transition regions from TCI to TI phases. (For interpretation of the colors in the figure, the reader is referred to the web version of this article.)

exclude the region from the phase diagram where the band consisting of p_z orbitals crosses the Fermi energy. In Fig. 3(a) and (b), energy gaps as a function of E_{p_z} are shown for bismuthene and antimonene, respectively. $E_{p_z} = -0.486$ eV ($E_{p_z} = -0.926$ eV) corresponds to freestanding bismuthene (antimonene), see Table 1, and $E_{p_z} = -10$ eV to structures deposited on the substrate (E_{p_x} and E_{p_y} energies are unchanged). TB model predicts bismuthene (antimonene) $E_{gap} \sim 0.9$ eV ($E_{gap} \sim 0.34$ eV), comparable with DFT results from Ref. [46] with structures on top of SiC under different tensile strain. Additionally, we show that weak coupling to the substrate is sufficient to observe a transition from TCI to TI phase, which occurs around $E_{p_z} \sim -2.5$ eV in both structures. After this phase transition, the energy gap is stable and only slightly affected by coupling strength with the substrate. Energy gap E_{gap} in bismuthene on the substrate ($E_{p_z} = -10$ eV) is almost three times larger than the gap in antimonene, compare energy scales in Fig. 3(a) and (b). This can be related to 2.5 times larger SOC strength in Bi (see Table 1). Energy gap of bismuthene on the substrate $E_{gap} = 0.9$ eV is also over three times larger than the energy gap of bismuth (111) bilayer, $E_{gap} = 0.25$ eV, which was noticed in Ref. [31].

We consider also a transition between bismuth (antimony) bilayer and bismuthene (antimonene) by applying additional strain for structures deposited on the substrate. The coupling to the SiC substrate of buckled structure is modeled by shifting the energy E_{p_z} of p_z for upper atom from a unit cell. The lower atom has the energy of p_z orbital $E_{p_z} = -10$ eV, as it is fully coupled to the substrate for all strain values. In Fig. 4(a) and (c) we show that bilayers deposited on a substrate are within a trivial insulator phase. It is observed that a small strain, around 1% for bismuth and 4% for antimony, induces a transition to TI phase. With stronger strain the energy gap monotonically increases to the largest value for flat systems, bismuthene and antimonene, corresponding to 20% strain in Fig. 4(a) and (c) respectively. In Fig. 4(b) and (d) we show corresponding band structures of systems in a ribbon geometry for 12.5% strain. A pair of edge states crosses the energy gap as expected for TI phase. The degeneracy of these edge states is removed due to inversion-symmetry breaking – two atoms from a unit cell are nonequivalent for a buckled structure as they couple differently to the substrate.

5. Entanglement spectra of Bi and Sb zigzag nanoribbons

To determine topological properties of Bi and Sb nanoribbons using entanglement spectrum, we divide the system into two equal spatial parts with a cut parallel to the physical edges [64]. ES corresponding to the one subsystem can be related to the energy

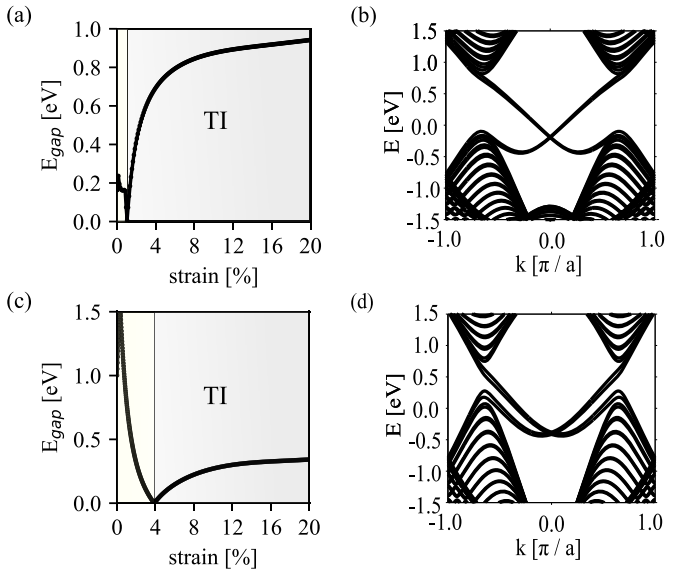

Fig. 4. Energy band gap E_{gap} as a function of strain for structures on the SiC substrate for (a) Bi and (c) Sb 2D crystals. In (a) and (c) topological phases are marked by different colors. (b) and (d) show the band structures of zigzag nanoribbon of Bi and Sb crystals within TI phase at 12.5% strain. Interaction with a substrate splits double degeneracy of each branch of edge states.

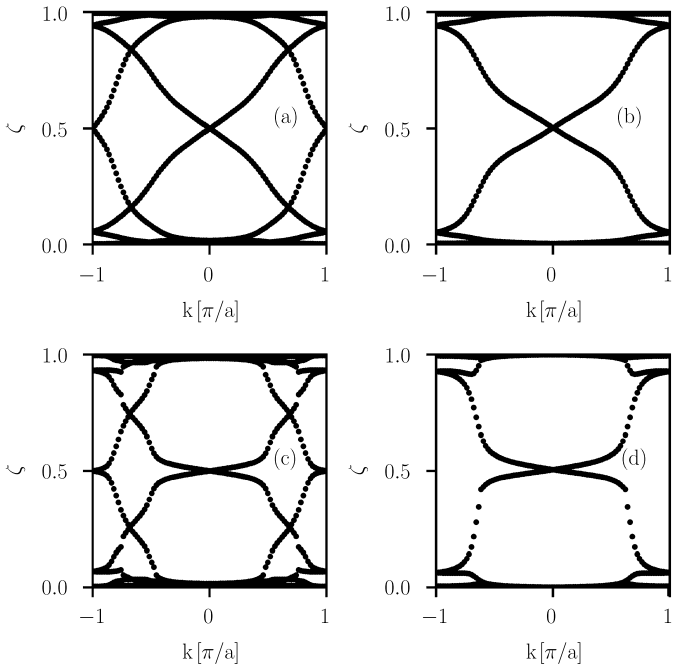

Fig. 5. Single-particle entanglement spectra of (a) bismuthene and (c) antimonene in a vacuum, which correspond to TCI phase. (b) Bi and (d) Sb bilayers on the substrate exhibit TI phase. One and two pairs of intersecting branches of edge states crossing the energy gap are characteristic features of TI and TCI phases, respectively.

spectrum of spectrally flattened Hamiltonian with open boundary conditions. Thus, ES can be compared with energy spectra of systems in a semi-infinite geometry, shown in Fig. 4(b) and (d) for TI phase and Fig. 6(a) and (c) for TCI phase.

In Fig. 5, we present the single-particle ES for (a) bismuthene and (c) antimonene in a vacuum. Two pairs of intersecting branches are exhibited, similarly to energy spectra from Fig. 6 in Section 6 and results from Ref. [8]. Spectral connection of 0's and 1's is the feature of a non-trivial phase and the number of branches distinguishes TCI and TI phases. Therefore, both entan-

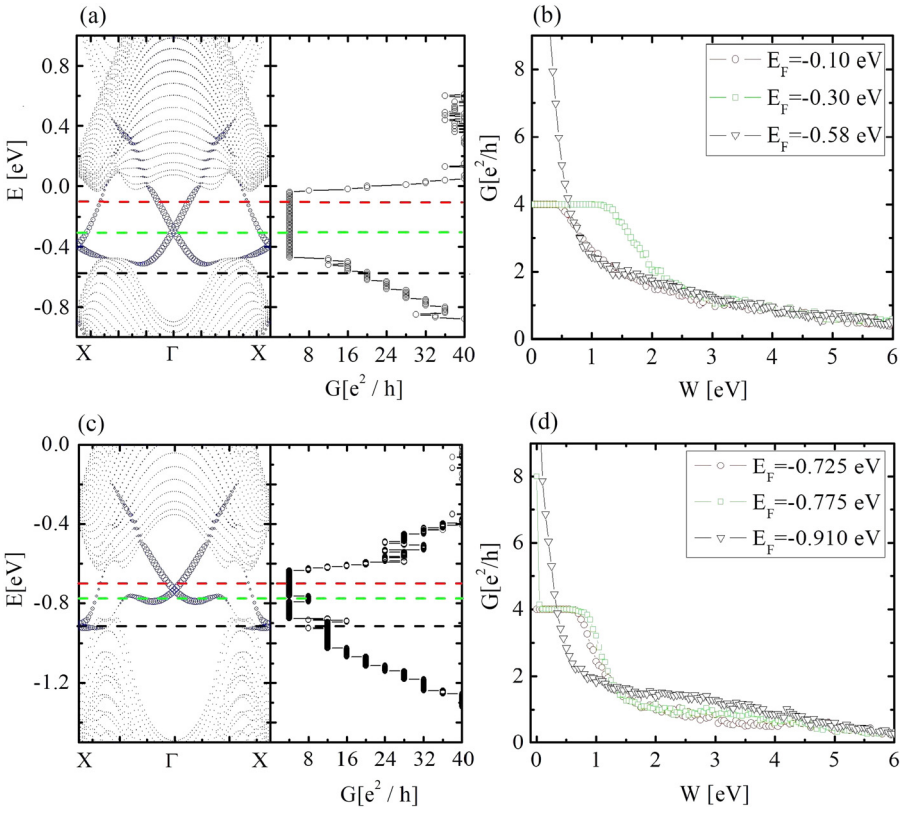

Fig. 6. Electronic and transport properties of freestanding (a, b) bismuthene and (c, d) antimonene nanoribbons in TCI phase. (a) and (c) Left: nanoribbon band structures in the first 1D Brillouin zone. Size of the blue circles represents level of localization of the wavefunction of a given state on the two atoms on both edges of the nanoribbon. Right: conductance G in clean system. (b, d) Conductance for three different Fermi energies, marked by horizontal color lines, as a function of the Anderson disorder strength W.

glement and energy spectra in a ribbon geometry can confirm existence of TCI phase. In Fig. 5 ES of (b) Bi and (d) Sb bilayers on a substrate are shown. Here, only one pair of modes spectrally connecting 0's and 1's is noticed (compare with energy spectra of ribbons in Fig. 4(b) and (d)). Thus, these systems are hosting TI phase.

6. Transport properties

Next, we focus on the topological protection of transport through edge states in zigzag-type nanoribbons of bismuthene and antimonene in a vacuum, corresponding to systems within TCI phase. In both bismuthene in Fig. 6(a) and antimonene in Fig. 6(c), we observe four branches of in-gap edge states with edge localization denoted by a size of blue circles. Edge states extend deeply into nanoribbon conduction band, which is novel with respect to previously studied Bi and Sb nanoribbons in TI region [32]. Transport in the clean samples with the Fermi energy E_F in the energy gap shows expected conductance equal to $4e^2/h$ for bismuthene. Antimonene edge states have nonlinear dispersion and eight edge states cross the Fermi level at some energies, e.g. around the Fermi energy $E_F \approx -0.8$ eV, Fig. 6(c). Fig. 6 (b) and (d) present results of transport calculations in the disorder samples for three different Fermi energies in both bismuthene and antimonene. For $E_F = -0.10$ eV in bismuthene in Fig. 6(b), one can observe protection against backscattering up to the disorder strength $W \approx 0.5$ eV. This critical value of W increases with the lowering of the Fermi energy to $E_F = -0.3$ eV and can be explained by a larger energetic distance to scattering channels from the conduction band states and a higher level of localization at the edges of the system, see larger blue circles in Fig. 6(a). A critical disorder strength W is smaller in a case of antimonene and can be related to nonlinear dispersion of edge states, together with possible scattering within edge channels and also to the smaller energy gap in comparison to bismuthene. Analogously to TI nanoribbons, we do not observe any protection against scattering for transport with Fermi energies within both conduction and valence bands, e.g. the latter case represented by $E_F = -0.58$ eV in Fig. 6(a) and $E_F = -0.91$ eV in Fig. 6(c). However, within the energy gap region, while Anderson type of disorder breaks a crystal symmetry, robust conductance is still expected.

7. Summary and discussion

To summarize, we have studied topological phases in Bi and Sb planar and buckled honeycomb crystals using multi-orbital TB method and compared the results with our and previous DFT calculations. TB model contains many hopping integrals that are chosen appropriately to fit to some ab initio method results. We have shown that a model with a parametrization from available literature is sufficient for a prediction of general features of the system, including its topological phases. We next used TB model to study systems on top of the substrate. We have shown that weak coupling to the substrate of buckled (but slightly strained) and planar crystals is sufficient to lead to a transition to Z_2 topological insulator phase. We have also proved that entanglement spectra can distinguish between TCI and TI phases which is revealed by two and one pair of branches of entanglement energies in a spectral flow, respectively. We have analyzed also TCI phase in the context of topological protection against scattering in transport through edge channels. Robust quantized conductance is observed even in the presence of crystal symmetry breaking Anderson-like disorder.

Acknowledgements

The authors acknowledge partial financial support from National Science Center (NCN), Poland, grant Maestro No. 2014/14/A/ST3/00654. Our calculations were performed in the Wrocław Center for Networking and Supercomputing.

References

[1] M.Z. Hasan, C.L. Kane, Colloquium: topological insulators, Rev. Mod. Phys. 82 (4) (2010) 3045.
[2] X.-L. Qi, S.-C. Zhang, Topological insulators and superconductors, Rev. Mod. Phys. 83 (4) (2011) 1057.
[3] L. Fu, C.L. Kane, Topological insulators with inversion symmetry, Phys. Rev. B 76 (4) (2007) 045302.
[4] Y. Ando, Topological insulator materials, J. Phys. Soc. Jpn. 82 (10) (2013) 102001.
[5] J.E. Moore, The birth of topological insulators, Nature 464 (7286) (2010) 194–198.
[6] L. Fu, Topological crystalline insulators, Phys. Rev. Lett. 106 (10) (2011) 106802.
[7] T.H. Hsieh, H. Lin, J. Liu, W. Duan, A. Bansil, L. Fu, Topological crystalline insulators in the SnTe material class, Nat. Commun. 3 (2012) 982.
[8] C.-H. Hsu, Z.-Q. Huang, C.P. Crisostomo, L.-Z. Yao, F.-C. Chuang, Y.-T. Liu, B. Wang, C.-H. Hsu, C.-C. Lee, H. Lin, et al., Two-dimensional topological crystalline insulator phase in Sb/Bi planar honeycomb with tunable Dirac gap, Sci. Rep. 6 (2016) 18993.
[9] S. Safaei, M. Galicka, P. Kacman, R. Buczko, Quantum spin Hall effect in IV–VI topological crystalline insulators, New J. Phys. 17 (6) (2015) 063041.
[10] J. Zhou, P. Jena, Two-dimensional topological crystalline quantum spin Hall effect in transition metal intercalated compounds, Phys. Rev. B 95 (8) (2017) 081102.
[11] P. Dziawa, B.J. Kowalski, K. Dybko, R. Buczko, A. Szczerbakow, M. Szot, E. Łusakowska, T. Balasubramanian, B.M. Wojek, M.H. Berntsen, O. Tjernberg, T. Story, Topological crystalline insulator states in $Pb_{1-x}Sn_xSe$, Nat. Mater. 11 (2012) 1023–1027.
[12] L.-Z. Yao, C.P. Crisostomo, C.-C. Yeh, S.-M. Lai, Z.-Q. Huang, C.-H. Hsu, F.-C. Chuang, H. Lin, A. Bansil, Predicted growth of two-dimensional topological insulator thin films of III–V compounds on Si (111) substrate, Sci. Rep. 5 (2015) 15463.
[13] B.A. Bernevig, S.-C. Zhang, Quantum spin Hall effect, Phys. Rev. Lett. 96 (10) (2006) 106802.
[14] C.L. Kane, E.J. Mele, Z2 topological order and the quantum spin Hall effect, Phys. Rev. Lett. 95 (14) (2005) 146802.
[15] C.L. Kane, E.J. Mele, Quantum spin Hall effect in graphene, Phys. Rev. Lett. 95 (22) (2005) 226801.
[16] C.-C. Liu, W. Feng, Y. Yao, Quantum spin Hall effect in silicene and two-dimensional germanium, Phys. Rev. Lett. 107 (7) (2011) 076802.
[17] M. König, S. Wiedmann, C. Brüne, A. Roth, H. Buhmann, L.W. Molenkamp, X.-L. Qi, S.-C. Zhang, Quantum spin Hall insulator state in HgTe quantum wells, Science 318 (5851) (2007) 766–770.
[18] C. Liu, T.L. Hughes, X.-L. Qi, K. Wang, S.-C. Zhang, Quantum spin Hall effect in inverted type-II semiconductors, Phys. Rev. Lett. 100 (23) (2008) 236601.
[19] I. Knez, R.-R. Du, G. Sullivan, Evidence for helical edge modes in inverted InAs/GaSb quantum wells, Phys. Rev. Lett. 107 (13) (2011) 136603.
[20] F.-C. Chuang, L.-Z. Yao, Z.-Q. Huang, Y.-T. Liu, C.-H. Hsu, T. Das, H. Lin, A. Bansil, Prediction of large-gap two-dimensional topological insulators consisting of bilayers of group III elements with Bi, Nano Lett. 14 (5) (2014) 2505–2508.
[21] C.P. Crisostomo, L.-Z. Yao, Z.-Q. Huang, C.-H. Hsu, F.-C. Chuang, H. Lin, M.A. Albao, A. Bansil, Robust large gap two-dimensional topological insulators in hydrogenated III–V buckled honeycombs, Nano Lett. 15 (10) (2015) 6568–6574.
[22] L. Li, X. Zhang, X. Chen, M. Zhao, Giant topological nontrivial band gaps in chloridized gallium bismuthide, Nano Lett. 15 (2) (2015) 1296–1301.
[23] M. Zhao, X. Chen, L. Li, X. Zhang, Driving a GaAs film to a large-gap topological insulator by tensile strain, Sci. Rep. 5 (2015) 8441.
[24] S. Murakami, Quantum spin Hall effect and enhanced magnetic response by spin–orbit coupling, Phys. Rev. Lett. 97 (23) (2006) 236805.
[25] M. Wada, S. Murakami, F. Freimuth, G. Bihlmayer, Localized edge states in two-dimensional topological insulators: ultrathin Bi films, Phys. Rev. B 83 (12) (2011) 121310.
[26] P.F. Zhang, Z. Liu, W. Duan, F. Liu, J. Wu, Topological and electronic transitions in a Sb(111) nanofilm: the interplay between quantum confinement and surface effect, Phys. Rev. B 85 (2012) 201410.
[27] Z.-Q. Huang, C.-H. Hsu, F.-C. Chuang, Y.-T. Liu, H. Lin, W.-S. Su, V. Ozolins, A. Bansil, Strain driven topological phase transitions in atomically thin films of group IV and V elements in the honeycomb structures, New J. Phys. 16 (10) (2014) 105018.
[28] I.K. Drozdov, A. Alexandradinata, S. Jeon, S. Nadj-Perge, H. Ji, R. Cava, B.A. Bernevig, A. Yazdani, One-dimensional topological edge states of bismuth bilayers, Nat. Phys. 10 (9) (2014) 664–669.
[29] N. Kawakami, C.-L. Lin, M. Kawai, R. Arafune, N. Takagi, One-dimensional edge state of Bi thin film grown on Si (111), Appl. Phys. Lett. 107 (3) (2015) 031602.
[30] F. Yang, L. Miao, Z. Wang, M.-Y. Yao, F. Zhu, Y. Song, M.-X. Wang, J.-P. Xu, A.V. Fedorov, Z. Sun, et al., Spatial and energy distribution of topological edge states in single Bi (111) bilayer, Phys. Rev. Lett. 109 (1) (2012) 016801.
[31] F. Reis, G. Li, L. Dudy, M. Bauernfeind, S. Glass, W. Hanke, R. Thomale, J. Schäfer, R. Claessen, Bismuthene on a SiC substrate: a candidate for a high-temperature quantum spin Hall material, Science 357 (6348) (2017) 287–290.
[32] M. Bieniek, T. Woźniak, P. Potasz, Stability of topological properties of bismuth (1 1 1) bilayer, J. Phys. Condens. Matter 29 (15) (2017) 155501.
[33] X. Li, H. Liu, H. Jiang, F. Wang, J. Feng, Edge engineering of a topological Bi(111) bilayer, Phys. Rev. B 90 (2014) 165412.
[34] Y.M. Koroteev, G. Bihlmayer, E.V. Chulkov, S. Blügel, First-principles investigation of structural and electronic properties of ultrathin Bi films, Phys. Rev. B 77 (2008) 045428.
[35] H. Pan, X.-S. Wang, Realization of Dirac cones in few bilayer Sb (111) films by surface modification, Nanoscale Res. Lett. 10 (1) (2015) 334.
[36] G. Bian, Z. Wang, X.-X. Wang, C. Xu, S. Xu, T. Miller, M.Z. Hasan, F. Liu, T.-C. Chiang, Engineering electronic structure of a two-dimensional topological insulator Bi (111) bilayer on Sb nanofilms by quantum confinement effect, ACS Nano 10 (3) (2016) 3859–3864.
[37] G. Cantele, D. Ninno, Size-dependent structural and electronic properties of Bi (111) ultrathin nanofilms from first principles, Phys. Rev. Mater. 1 (1) (2017) 014002.
[38] P. Potasz, J. Fernández-Rossier, Orbital magnetization of quantum spin Hall insulator nanoparticles, Nano Lett. 15 (9) (2015) 5799–5803, pMID: 26252612.
[39] R.R.Q. Freitas, R. Rivelino, F. de Brito Mota, C.M.C. de Castilho, A. Kakanakova-Georgieva, G.K. Gueorguiev, Topological insulating phases in two-dimensional bismuth-containing single layers preserved by hydrogenation, J. Phys. Chem. C 119 (41) (2015) 23599–23606.
[40] M. Bieniek, T. Woźniak, P. Potasz, Study of spin–orbit coupling effect on bismuth (111) bilayer, Acta Phys. Pol. A 130 (2) (2016) 609–612.
[41] K.-H. Jin, S.-H. Jhi, Quantum anomalous Hall and quantum spin-Hall phases in flattened Bi and Sb bilayers, Sci. Rep. 5 (2015) 8426.
[42] F.-C. Chuang, C.-H. Hsu, C.-Y. Chen, Z.-Q. Huang, V. Ozolins, H. Lin, A. Bansil, Tunable topological electronic structures in Sb (111) bilayers: a first-principles study, Appl. Phys. Lett. 102 (2) (2013) 022424.
[43] Z.-Q. Huang, F.-C. Chuang, C.-H. Hsu, Y.-T. Liu, H.-R. Chang, H. Lin, A. Bansil, Phys. Rev. B 88 (2013) 165301.
[44] S. Singh, A.C. Garcia-Castro, I. Valencia-Jaime, F. Muñoz, A.H. Romero, Prediction and control of spin polarization in a Weyl semimetallic phase of BiSb, Phys. Rev. B 94 (2016) 161116.
[45] Z.-Q. Huang, F.-C. Chuang, C.-H. Hsu, Y.-T. Liu, H.-R. Chang, H. Lin, A. Bansil, Nontrivial topological electronic structures in a single Bi (111) bilayer on different substrates: a first-principles study, Phys. Rev. B 88 (16) (2013) 165301.
[46] C.-H. Hsu, Z.-Q. Huang, F.-C. Chuang, C.-C. Kuo, Y.-T. Liu, H. Lin, A. Bansil, The nontrivial electronic structure of Bi/Sb honeycombs on SiC (0001), New J. Phys. 17 (2) (2015) 025005.
[47] C.-C. Liu, S. Guan, Z. Song, S.A. Yang, J. Yang, Y. Yao, Low-energy effective hamiltonian for giant-gap quantum spin Hall insulators in honeycomb X-hydride/halide (X = N–Bi) monolayers, Phys. Rev. B, Condens. Matter 90 (8) (2014) 085431.
[48] T. Hirahara, N. Fukui, T. Shirasawa, M. Yamada, M. Aitani, H. Miyazaki, M. Matsunami, S. Kimura, T. Takahashi, S. Hasegawa, K. Kobayashi, Phys. Rev. Lett. 109 (2012) 227401.
[49] Z. Liu, C.-X. Liu, Y.-S. Wu, W.-H. Duan, F. Liu, J. Wu, Phys. Rev. Lett. 107 (2011) 136805.
[50] Y. Liu, R.E. Allen, Electronic structure of the semimetals Bi and Sb, Phys. Rev. B 52 (3) (1995) 1566.
[51] J.C. Slater, G.F. Koster, Simplified LCAO method for the periodic potential problem, Phys. Rev. 94 (1954) 1498–1524.
[52] D. Chadi, Spin–orbit splitting in crystalline and compositionally disordered semiconductors, Phys. Rev. B 16 (2) (1977) 790.
[53] Z. Liu, C.-X. Liu, Y.-S. Wu, W.-H. Duan, F. Liu, J. Wu, Stable nontrivial Z2 topology in ultrathin Bi (111) films: a first-principles study, Phys. Rev. Lett. 107 (13) (2011) 136805.
[54] J.P. Perdew, K. Burke, M. Ernzerhof, Generalized gradient approximation made simple, Phys. Rev. Lett. 77 (18) (1996) 3865.
[55] H.J. Monkhorst, J.D. Pack, Special points for Brillouin-zone integrations, Phys. Rev. B 13 (12) (1976) 5188.
[56] P. Giannozzi, S. Baroni, N. Bonini, M. Calandra, R. Car, C. Cavazzoni, D. Ceresoli, G.L. Chiarotti, M. Cococcioni, I. Dabo, A.D. Corso, S. de Gironcoli, S. Fabris, G. Fratesi, R. Gebauer, U. Gerstmann, C. Gougoussis, A. Kokalj, M. Lazzeri, L. Martin-Samos, N. Marzari, F. Mauri, R. Mazzarello, S. Paolini, A. Pasquarello, L. Paulatto, C. Sbraccia, S. Scandolo, G. Sclauzero, A.P. Seitsonen, A. Smogunov, P. Umari, R.M. Wentzcovitch, Quantum Espresso: a modular and open-source software project for quantum simulations of materials, J. Phys. Condens. Matter 21 (39) (2009) 395502.
[57] O.Ü. Aktürk, V.O. Özçelik, S. Ciraci, Single-layer crystalline phases of antimony: antimonenes, Phys. Rev. B 91 (23) (2015) 235446.

[58] E. Aktürk, O.Ü. Aktürk, S. Ciraci, Single and bilayer bismuthene: stability at high temperature and mechanical and electronic properties, Phys. Rev. B 94 (1) (2016) 014115.
[59] H. Li, F.D.M. Haldane, Entanglement spectrum as a generalization of entanglement entropy: identification of topological order in non-abelian fractional quantum Hall effect states, Phys. Rev. Lett. 101 (2008) 010504.
[60] I. Peschel, Calculation of reduced density matrices from correlation functions, J. Phys. A, Math. Gen. 36 (14) (2003) L205.
[61] A. Alexandradinata, T.L. Hughes, B.A. Bernevig, Trace index and spectral flow in the entanglement spectrum of topological insulators, Phys. Rev. B 84 (2011) 195103.
[62] T.L. Hughes, E. Prodan, B.A. Bernevig, Inversion-symmetric topological insulators, Phys. Rev. B 83 (2011) 245132.
[63] A.M. Turner, Y. Zhang, A. Vishwanath, Entanglement and inversion symmetry in topological insulators, Phys. Rev. B 82 (2010) 241102.
[64] M. Brzezińska, M. Bieniek, T. Woźniak, P. Potasz, A. Wójs, Entanglement entropy and entanglement spectrum of $Bi_{1-x}Sb_x$ (1-1-1) bilayers, J. Phys. Condens. Matter 30 (12) (2018) 125501.